Temporomandibular joint loading patterns related to joint morphology: a theoretical study

Colombo, V ; Palla, S ; Gallo, L M

Abstract: It is unclear which aspects of the temporomandibular joint (TMJ) anatomy and/or kinematics determine shape and location of disk-compressive areas (stress field). The aim of this study was a quantitative analysis of TMJ anatomy to predict stress field path direction. Twenty-five asymptomatic TMJs (12 females and 13 males, aged 20-38 years) were tracked during unloaded opening/closing cycles. All TMJs were magnetic resonance (MR) imaged, reconstructed and animated with the recorded kinematics. Quantitative morphological parameters were calculated and entered into cross-validated multivariate discriminant analysis. Stress field paths during jaw opening were classified as mediolateral (ML) in 14 (9 females and 5 males) and lateromedial (LM) in 11 joints (3 females and 8 males). Curvature and incongruence as well as the dorsoventral position of the condyle in the fossa showed statistically significant differences (Mann-Whitney U test, $p < 0.05$). A combination of the lateral incongruence, the distance from the posterior slope of the eminence as well as the maximum posterior sagittal curvature enabled to correctly predict the direction of stress field paths in 92% of cases. In particular, ML type joints had laterally more congruent condyles/fossae and condyles more distant from the posterior slope of the eminence than LM type joints. Within the limits of this study, TMJ morphology seems to determine stress field path patterns.

DOI: https://doi.org/10.1159/000113408

Original Paper

Cells Tissues Organs

Cells Tissues Organs 2008;187:295–306
DOI: 10.1159/000113408

Accepted after revision: September 11, 2007
Published online: January 14, 2008

Temporomandibular Joint Loading Patterns Related to Joint Morphology: A Theoretical Study

Vera Colombo Sandro Palla Luigi M. Gallo

Clinic for Masticatory Disorders and Complete Dentures, Center for Oral Medicine, Dental and Maxillofacial Surgery, University of Zurich, Zurich, Switzerland

Key Words
Biomechanics · Functional anatomy · Kinematics · Temporomandibular disorders · Temporomandibular joint

Abstract
It is unclear which aspects of the temporomandibular joint (TMJ) anatomy and/or kinematics determine shape and location of disk-compressive areas (stress field). The aim of this study was a quantitative analysis of TMJ anatomy to predict stress field path direction. Twenty-five asymptomatic TMJs (12 females and 13 males, aged 20–38 years) were tracked during unloaded opening/closing cycles. All TMJs were magnetic resonance (MR) imaged, reconstructed and animated with the recorded kinematics. Quantitative morphological parameters were calculated and entered into cross-validated multivariate discriminant analysis. Stress field paths during jaw opening were classified as mediolateral (ML) in 14 (9 females and 5 males) and lateromedial (LM) in 11 joints (3 females and 8 males). Curvature and incongruence as well as the dorsoventral position of the condyle in the fossa showed statistically significant differences (Mann-Whitney U test, $p < 0.05$). A combination of the lateral incongruence, the distance from the posterior slope of the eminence as well as the maximum posterior sagittal curvature enabled to correctly predict the direction of stress field paths in 92% of cases. In particular, ML type joints had laterally more congruent condyles/fossae and condyles more distant from the posterior slope of the eminence than LM type joints. Within the limits of this study, TMJ morphology seems to determine stress field path patterns.

Introduction

The study of joint biomechanics is important because dysfunction and breakdown of joint components seem to be, at least partially, of mechanical origin. Diarthrodial joints, such as the knee and the temporomandibular joint (TMJ), have been the topic of extensive research due to the impact of their pathologies on everyday activities, such as gait and orofacial function. Both joint types share several characteristics, e.g. kinematics with six degrees of freedom, high incongruence of the articular surfaces, presence of fibrocartilaginous menisci and the effect of unilateral dysfunction on the contralateral joint. A thorough understanding of the pathomechanisms of degenerative joint diseases, i.e. osteoarthritis, of these types of joints needs to consider kinematic function, bone and

KARGER

Fax +41 61 306 12 34
E-Mail karger@karger.ch
www.karger.com

1422–6405/08/1874–0295$24.50/0

Accessible online at:
www.karger.com/cto

Prof. Luigi M. Gallo
Plattenstrasse 11
CH–8032 Zurich (Switzerland)
Tel. +41 44 634 3226, Fax +41 44 634 4302
E-Mail luigi@zui.uzh.ch

Abbreviations used in this paper

CAP	point on the anterior part of a condylar sagittal section
CCP	center of the condyle on a sagittal slice
CGP_i	one of 17 points equidistantly set on the cranial part of the condylar coronal contour
$C\kappa_{Ci}$	curvature value of the condyle
$C\kappa_{Cmax}$	maximum curvature of the condyle
$C\kappa_{Fi}$	curvature value of the fossa
CLP	lateral pole of the condyle
CMP	medial pole of the condyle
$C\sigma_{Ai}$	anterior curvature of the condyle
$C\sigma_{Ai,j}$	anterior condylar curvature values
$C\sigma_{Amax}$	maximum of the anterior curvatures of the condyle
$C\sigma_{Pi}$	posterior curvature of the condyle
$C\sigma_{Pi,j}$	posterior condylar curvature values
$C\sigma_{Pmax}$	maximum posterior condylar curvature in the sagittal sections
$C\tau_{Ai}$	curvature value of the anterior condylar arch
$C\tau_{Amax}$	maximum anterior curvature of the condyle
$C\tau_{Pi}$	curvature value of the posterior condylar arch
CTP	condylar top point
d_{CFi}	distances between condyle and fossa
$d\kappa_{CFi}$	point at a distance between FGP_i and CGP_i
$d\kappa_{ML}$	distance between the lateral and medial condylar poles
$d\sigma_{ACF}$	anterior distance between condyle and fossa, calculated between the points CAP and FAP
$d\sigma_{ACFC}$	distance $d\sigma_{ACFj}$ averaged on the two central sagittal sections
$d\sigma_{ACFj}$	distance between the anterior face of the condyle and the fossa
$d\sigma_{ACFL}$	distance $d\sigma_{ACFj}$ averaged on the two lateral sagittal sections
$d\sigma_{ACFM}$	distance $d\sigma_{ACFj}$ averaged on the two medial sagittal sections
$d\sigma_{ACFmin}$	closest condyle-fossa distance $d\sigma_{ACF\,min}$
$d\sigma_{PCF}$	posterior distance between condyle and fossa, calculated between the points FPP and CPP
FAP	point on the anterior part of a fossa sagittal section
FCP_{max}	steepest point of the fossa contour between its most cranial point
FCP_{min}	steepest point of the fossa contour between its most caudal point
FGP_i	one of 17 points equidistantly set on the fossa coronal contour
FPP	point on the posterior part of a fossa sagittal section
FSP	steepest point of the fossa contour
$G\kappa_{CF\,17}$	incongruence between condyle and fossa in the most lateral part of the joints
$G\kappa_{CFC}$	incongruence between the central parts of condyle and fossa
$G\kappa_{CFi}$	incongruence between condyle and fossa at each point couple CGP_i and FGP_i
$G\kappa_{CFL}$	incongruence between the lateral parts of condyle and fossa
$G\kappa_{CFM}$	incongruence between the medial parts of condyle and fossa
κ	coronal plane
LM	lateromedial
ML	mediolateral
MR	magnetic resonance
σ	sagittal plane
$S\sigma_{avg}$	average of the values of the slopes of the fossa over all sagittal sections
$S\sigma_j$	slope of the fossa
τ	transversal plane
TMJ	temporomandibular joint

cartilage morphology and biological response [Andriacchi et al., 2004]. The accurate analysis of the relationship between the joint articular surfaces permits the assessment of contact and compression areas and therefore the strains and stresses undergone by soft and hard tissues that might lead to osteoarthritis. This could help identifying subjects at risk of developing cartilage degeneration. It could also help tissue engineers to design parts able to withstand realistic tissue deformations. Several studies simulated or measured the cartilage loading patterns under static conditions in the knee [Fujikawa et al., 1983; Ateshian et al., 1994] as well as in the TMJ [Beek et al., 2001; Tanaka et al., 2004; Hirose et al., 2006]. Nowadays, it is recognized that the mechanism of cartilage loading and degeneration needs to be addressed also dynamically and activity dependent [Andriacchi et al., 2000, 2003]. The methods developed at our clinic for jaw tracking [Mesqui et al., 1986; Airoldi, 1994; Gallo et al., 1997, 2000a] and for combining magnetic resonance (MR) images with jaw motion [Krebs et al., 1995; Krebs, 1997; Fushima et al., 2003; Palla et al., 2003] provide a highly accurate dynamic insight into the TMJ articular space. This method has been used to demonstrate that during unloaded mandibular movements mediolateral (ML) stress field translation occurs in the TMJ disk and that in 65% of 48 TMJs from 30 asymptomatic subjects the stress field paths moved in an ML pattern (fig. 1a) and in 20% in a lateromedial (LM) one (fig. 1b), the majority of the joints being laterally exposed to higher stress field translation velocities [Gallo et al., 2000b, 2001]. Tractional forces parallel to the joint surfaces result from frictional and plowing forces [Linn, 1967]. Whereas frictional forces have been shown to be very low [Nickel and McLachlan, 1994b], the plowing forces, i.e. the tangential forces due to the displacement of compressive deformation through the cartilage matrix, resulting from stress field translation [Waldman and Bryant, 1997] might contribute to TMJ disk damage since this tissue is less resis-

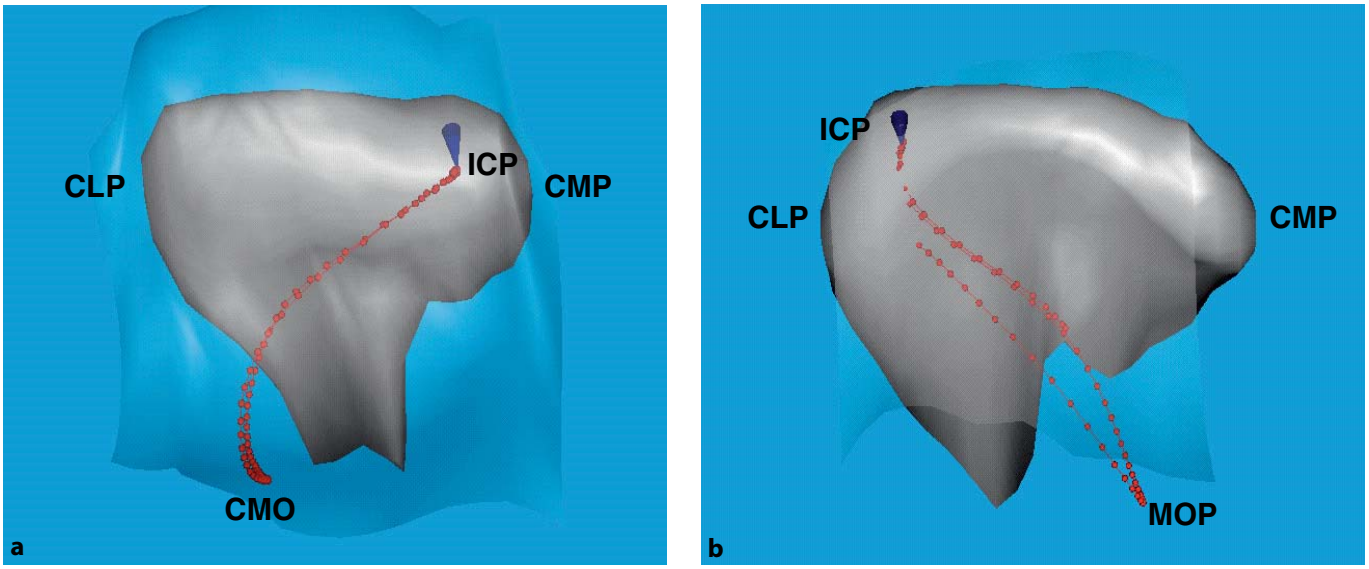

Fig. 1. Example of the two types of TMJ stress field paths at jaw opening. **a** ML group. **b** LM group. The red trace represents the stress field path during jaw opening/closing and the blue cone represents the actual position of the stress field centroid with the mandible in intercuspal position. ICP = Position at maximum intercuspation; MOP = maximum opening position.

tant to forces directed ML than to those directed dorsoventrally [Beatty et al., 2001]. These studies also led to the hypothesis that the higher mechanical work produced by plowing found in some joints might identify subjects at risk for disk fatigue that could increase the likelihood of osteoarthritis [Nickel and McLachlan, 1994a; Nickel et al., 2001]. Furthermore, ML stress field translation in clicking TMJs during jaw opening/closing is significantly larger than in asymptomatic joints, and the stress field paths are non-coincident during the opening/closing phases [Gossi et al., 2004]. This study also suggested that in clicking TMJs the minimum intra-articular distance is smaller than in controls, which could imply a thinning of the disk and a flattening of the bony surfaces. These results are consistent with the observations of diskal and condylar remodeling in static MR images in clicking TMJs [Rao et al., 1990; Chen et al., 2002]. Since most deformed disks analyzed in these works were stretched laterally, it is reasonable to hypothesize that the location and the characteristics of stress field translation might influence the location of disk damage. To date it is unknown which aspects of TMJ anatomy and kinematics affect the stress field patterns during function. The aim of this study was therefore to analyze quantitatively whether TMJ morphology affects the direction of the stress field paths during unloaded jaw opening/closing movements.

Patients and Methods

Subjects

The data from 16 healthy subjects (9 males and 7 females, 20–38 years of age), for a total of 25 normal TMJs (determined by history and clinical examination), were analyzed. The subjects were selected from our clinic charts. Potential subjects had been interviewed in order to exclude a myoarthropathy of the masticatory system or other diseases according to the clinic's protocol: pain or sounds in the TMJ, pain or fatigue in the masticatory muscles, impaired jaw mobility, facial pain, headache and toothache, with details being given in previous studies [Palla, 1986; Salaorni and Palla, 1994]. Subjects with a negative history underwent a clinical examination: measurement of active and passive mandibular mobility; palpation and auscultation of the TMJs, and palpation of masticatory, neck and shoulder muscles [for details, see Gallo et al., 1997]. Inclusion criteria were: maximum opening >40 mm (overbite included), mandibular deviation and/or deflection on opening/closing <2 mm, protrusion and laterotrusion >7 mm, difference between active and passive maximum opening <2 mm, and absence of tenderness to palpation of the TMJ area and masticatory as well as neck muscles [Palla, 1986]. Wear facets were accepted, provided the provocation test was negative [Krogh-Poulsen, 1973]. An informed verbal consent to participate in the study was obtained from all subjects. The study protocol was approved by the University of Zurich Institutional Review Board. Care was taken to have almost the same number of ML and LM stress field patterns according to the method of a previous study [Gallo et al., 2001]. Of the 25 TMJs, 14 (9 belonging to females and 5 belonging to males) had a stress field path running ML whereas 11 (3 belonging to females and 8 belonging to males) had a LM stress field path during jaw opening. The mean age of the subjects

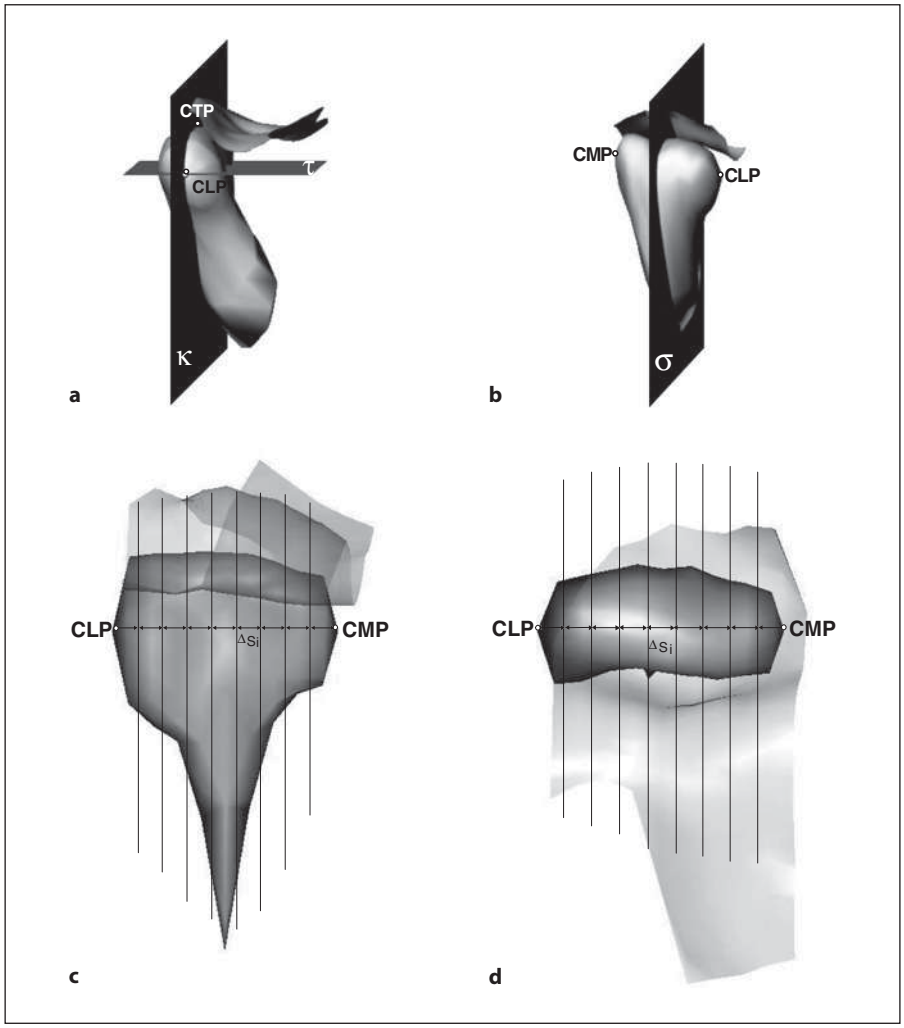

Fig. 2. Reference planes for the morphological analysis. κ, τ and σ = Coronal, transversal and sagittal planes, respectively; ΔS_i = distance between two contiguous sagittal sections out of the eight equidistantly set through the condyle. For the definition of the planes, see the text.

did not differ between the two pattern types, however, significantly more females had an ML pattern and significantly more males an LM pattern according to a χ^2 test ($p < 0.05$).

Reconstruction and Animation of the TMJ

For reconstruction and animation (*dynamic stereometry)* of the TMJ, anatomic software models from MR imaging were coupled with the real kinematic data of each joint. MR scans, consisting of 14 sagittal views made perpendicular to the condylar long axis, were recorded by means of a 1.5-Tesla system (Gyroscan ACS-II; Philips Medical System, Best, The Netherlands) with the subject biting on a monobloc. This was rigidly connected to an external frame reference system, which served to transform the MR coordinates into those of the jaw tracker. This consisted of three linear cameras recording the relative temporospatial changes of two sets of three light-emitting diodes attached to mandibular and maxillary teeth [Mesqui et al., 1986; Airoldi et al., 1994]. The MR images were segmented by means of an interactive line editor to obtain the contours of the mandibular condyle and fossa that were then joined into wire frames representing the articulating surfaces [Krebs et al., 1995; Krebs, 1997; Gossi et al., 2004]. Motion data were applied to the reconstructed anatomical structures by means of custom-written software running on a Windows™ personal computer. Errors in the method have been reported previously [Krebs, 1997] and are within the range of 1 mm.

Experimental Procedure

The study protocol required first the MR recording. At a subsequent visit, jaw movement was recorded for each subject using the jaw tracker while performing 10 cycles of symmetric jaw opening/closing from maximum intercuspation to maximum opening paced at 1 Hz. For each joint, jaw tracking was performed on the ipsilateral side in order to minimize geometric noise [Airoldi et al., 1994].

Data Analysis

The center of the stress field was approximated as the area of minimum condyle-fossa distance [Nickel and McLachlan, 1994c; Gossi et al., 2004]. Therefore, for each sampling time of mandibular motion, the 30 smallest adjacent condyle-fossa distances, mea-

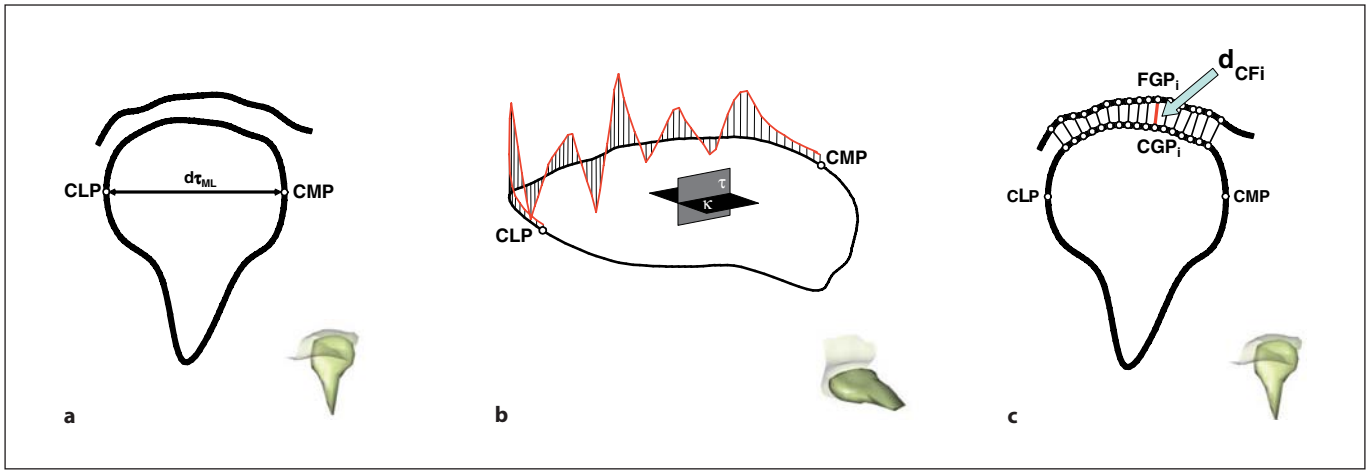

Fig. 3. Quantitative parameters describing the TMJ anatomy in the coronal plane. **a** Intracondylar distance $d\kappa_{ML}$ between the condylar poles CMP and CLP. $d\tau_{ML}$ = Distance between the condylar poles. **b** Curvature values $C\kappa_{Ci}$ along the cranial part of the condyle contour between the condylar poles; the curvature values $C\kappa_{Fi}$ along the fossa contour are determined in a similar way. **c** Incongruence values $G\kappa_{CFi}$ between condyle and fossa. For a detailed definition of the parameters, see the text.

sured between polygon vertices, were identified. The centroid of the area defined by these 30 minimum distances was calculated and determined the position of the stress field. The components of the position of the stress field were smoothed by uniform averaging of the values sampled over 84 ms. The anatomical features were analyzed with the mandible at maximum intercuspation by first choosing reference planes in every TMJ according to anatomic landmarks. The *coronal plane* κ was defined as the plane running through the medial (CMP) and lateral pole (CLP) of the condyle, and the top point of the condyle (CTP; fig. 2a), the *transversal plane* τ through the condylar poles and perpendicular to the coronal plane (fig. 2a) and the *sagittal plane* σ perpendicular to κ and τ (fig. 2b). Eight further sagittal planes were then uniformly spaced through the condyle (fig. 2c, d). Sections of condyle and fossa were obtained by intersecting the wire frame with the eight planes defined. These sections were then interpolated by means of splines that allowed determining normals, tangents and curvatures of the sections. Note that the reference planes used do not exactly coincide with the anatomical planes, they are slightly angulated according to the condylar orientation. The names of the reference planes have been chosen for the sake of simplicity. The morphological description of the TMJs was performed considering anatomical features that likely create compressive areas, in particular the curvature of the articular surfaces. For instance, a more curved convex surface (condyle) could create a compression area if pushed against a less curved concave surface (fossa). For the same reason, further parameters describe the intra-articular distances, the incongruence (similarity) of the articular surfaces, as well as the steepness of the fossa that could also cause a compression if steeper and thus closer to the moving condyle.

Therefore, the following parameters were calculated in the different planes and sections in order to describe the shapes of condyle and fossa and their relationship.

Coronal Plane κ

The *distance between the* CMP and CLP ($d\kappa_{ML}$) was a measure of the condylar width (fig. 3a).

Curvature along the Superior Arch of Condyle and Fossa. Twenty equidistant points were chosen along the cranial part of the condylar contour between CMP and CLP as well as along the fossa contour (fig. 3b). The curvature values of the condyle ($C\kappa_{Ci}$) and of the fossa ($C\kappa_{Fi}$; i = 1–20) were determined for each point and were expressed per millimeter, being the inverse of the radius of the curvature in each point. The curvature was therefore zero for a straight segment, positive for a convex and negative for a concave segment. For data reduction purposes, we considered the maximum curvature of the condyle $C\kappa_{Cmax}$.

Incongruence between Condyle and Fossa. For this parameter, we utilized a previously described method [Nickel and McLachlan, 1994a]. Along the cranial part of the condylar contour we determined a set of 17 points CGP_i (i = 1–17) by dividing the intracondylar axis (the straight segment between CMP and CLP) into 18 equal intervals and by projecting them onto the condylar contour (fig. 3c). Therefore, the condylar poles CMP and CLP were not considered. For each point CGP_i we drew the straight line, normal to the condyle, that intersected the fossa in a point FGP_i at distance $d\kappa_{CFi}$ from CGP_i. For each pair of points (one on the condyle and one on the fossa) the local incongruence $G\kappa_{CFi}$ was determined according to the formula:

$$G\kappa_{CFi} = d_{CFi} - \frac{1}{n}\sum_{i=1}^{n} d_{CFi}.$$

The incongruence was 0 mm for congruent contours (i.e. with the same shape), <0 for distances between condyle and fossa smaller than their overall average d_{CFi} and >0 for distances between condyle and fossa larger than average. For data reduction purposes, the incongruence was averaged on the three lateral, central and medial sections, thus yielding the parameters $G\kappa_{CFL}$, $G\kappa_{CFC}$ and $G\kappa_{CFM}$.

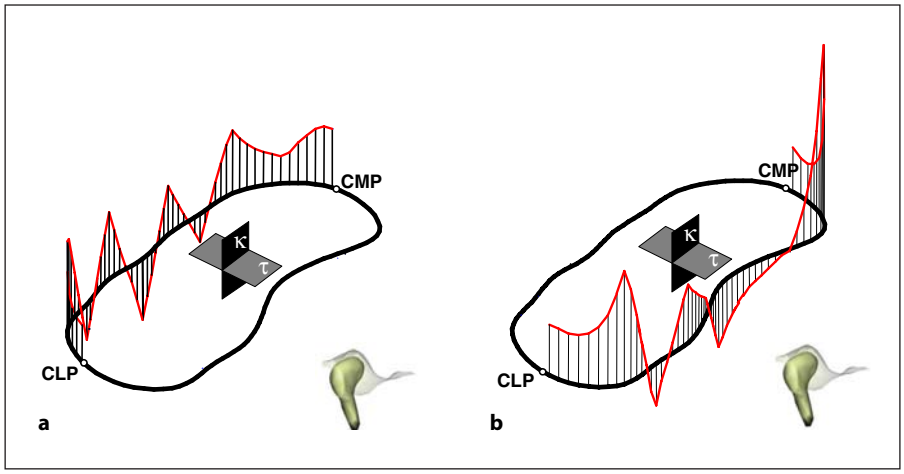

Fig. 4. Quantitative parameters describing TMJ anatomy in the transversal plane. Curvature values $C\tau_{Ai}$ of the anterior (**a**) and $C\tau_{Pi}$ of the posterior condylar arch (**b**). For a detailed definition of the parameters, see the text.

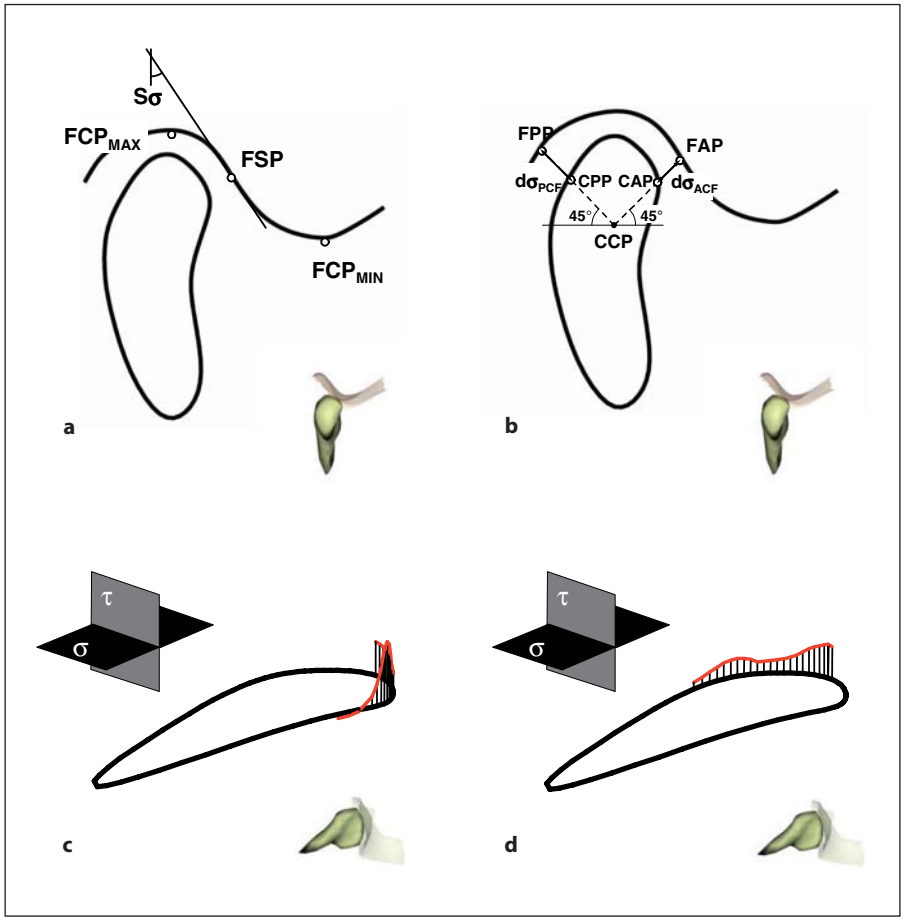

Fig. 5. Quantitative parameters describing TMJ anatomy on each sagittal section. **a** Slope of the fossa $S\sigma_i$, i.e. the angle of the tangent to the steepest point (FSP) of the fossa contour between its most cranial (FCP_{max}) and its most caudal point (FCP_{min}). **b** Anterior distance $d\sigma_{ACF}$ between condyle and fossa, calculated between the points CAP and FAP. **c** Anterior curvature $C\sigma_{Ai}$ of the condyle. **d** Posterior curvature $C\sigma_{Pi}$ of the condyle. For a detailed definition of the parameters, see the text.

Transversal Plane τ

Curvature of the Anterior and Posterior Condylar Arch. Similarly to the coronal plane, 20 equidistant points were chosen along the anterior part of the condylar contour between CMP and CL, and the curvature value of the anterior contour ($C\tau_{Ai}$; i = 1–20) was determined for each point (fig. 4a, b). The same was done for the values along the posterior part of the condylar contour ($C\tau_{Pi}$, i = 1–20). For data reduction purposes, we considered the maximum anterior curvature of the condyle $C\tau_{Amax}$.

Sagittal Sections σi

Slope of the Fossa. The slope of the fossa $S\sigma_j$ (j = 1–8) was defined on each sagittal section as the angle between the tangent to the steepest point of the fossa contour between its most cranial and its most caudal point and the coronal plane (fig. 5a). For data reduction purposes, we then considered the average of the values of the slopes of the fossa over all sagittal sections $S\sigma_{avg}$.

Distance between the Anterior Face of the Condyle and Fossa. The center of the condyle was defined on each section as lying on the intersection of (a) the plane κ_1 running through CTP and (b) the transversal plane τ. The distance between the anterior face of the condyle and the fossa $d\sigma_{ACFj}$ (j = 1–8) was determined on the line 45° from the line connecting the condylar center and apex (fig. 5b). For data reduction purposes, the distance $d\sigma_{ACFj}$ was averaged on the two lateral, central and medial sagittal sections, thus yielding the parameters $d\sigma_{ACFL}$, $d\sigma_{ACFC}$ and $d\sigma_{ACFM}$, respectively.

Curvature of the Anterior and Posterior Condylar Contour. The anterior and posterior condylar curvature values $C\sigma_{Ai,j}$ and $C\sigma_{Pi,j}$ (i = 1–20 and j = 1–8) were determined for each of the 20 equally spaced points on the anterior and posterior condylar portion of each of the eight sagittal sections. (fig. 5c). For data reduction purposes, we considered only the maximum of the anterior curvatures of the condyle $C\sigma_{Amax}$ averaged on each section.

Statistical Analysis

Univariate analyses of the parameters (i.e. $C\kappa_{Cmax}$, $G\kappa_{CFL}$, $G\kappa_{CFC}$, $G\kappa_{CFM}$, $C\tau_{Amax}$, $S\sigma_{avg}$, $d\sigma_{ACFL}$, $d\sigma_{ACFC}$, $d\sigma_{ACFM}$ and $C\sigma_{Amax}$) were performed by means of nonparametric Wilcoxon-Mann-Whitney tests between the ML and LM groups (SPSS™ 12.0.1 for Windows). Furthermore, a multivariate discriminant analysis (Statgraphics Centurion XV™) was performed on all parameters determined. This is an algorithm that helps to predict the class based on the influence of the different parameters on the classification of the two types of stress field patterns.

Table 1. Demographic data, classification of the stress field paths and distance between the medial and lateral poles (condyle width $d\kappa_{ML}$)

Subject		Age years	TMJ, No.		Path		Condyle width $d\kappa_{ML}$, mm	
No.	gender		left	right	left	right	left	righ
1	M	32		1		LM		18.2
2	M	28	2		LM		20.3	
3	M	31		3		LM		20.9
4	F	38	4	5	ML	ML	16.6	16.3
5	F	28	6	7	ML	ML	16.6	16.7
6	M	29	8	9	LM	LM	18.9	20.7
7	M	36	10	11	LM	ML	16.6	18.8
8	F	24	12	13	LM	LM	16.6	17.0
9	M	23	14	15	ML	ML	14.8	14.4
10	M	24	16		LM		16.3	
11	F	20	17	18	ML	ML	13.2	14.5
12	F	27	19		LM		16.6	
13	F	31	20	21	ML	ML	20.5	18.7
14	F	22		22		ML		14.5
15	M	24	23	24	ML	ML	16.3	16.7
16	M	26	25		LM		18.6	

Results

Table 2 shows the medians as well as the first and third quartiles of the parameters summarizing TMJ morphology as well as the p values of the statistical tests between the groups with stress fields running in an ML and LM pattern during unloaded jaw opening. The distance be-

Table 2. Parameters describing TMJ morphology in the three planes and p values according to the Mann-Whitney test

	Parameters		ML	LM	p
κ	$C\kappa_{Cmax}$	mm^{-1}	0.8 (0.6; 0.9)	0.6 (0.5; 0.8)	0.380
	$G\kappa_{CFM}$	mm	–0.2 (–0.8; –0.1)	–0.0 (–0.6; 0.3)	0.324
	$G\kappa_{CFC}$	mm	0.2 (–0.2; 0.4)	0.2 (0.0; 0.3)	0.622
	$G\kappa_{CFL}$	mm	–0.4 (–0.6; 0.4)	–1.1 (–1.1; –0.6)	0.003
τ	$C\tau_{Amax}$	mm^{-1}	0.8 (0.7; 1.0)	0.9 (0.7; 1.0)	0.891
σ	$S\sigma_{avg}$	°	26.8 (14.8; 35.0)	28.8 (20.9; 32.0)	0.848
	$d\sigma_{ACFM}$	mm	3.1 (2.6; 4.4)	3.4 (3.2; 4.4)	0.239
	$d\sigma_{ACFC}$	mm	3.2 (2.3; 4.2)	3.5 (2.7; 4.6)	0.412
	$d\sigma_{ACFL}$	mm	3.5 (2.5; 4.2)	2.3 (2.1; 2.3)	0.004
	$C\sigma_{Amax}$	mm^{-1}	0.4 (0.38; 0.49)	0.37 (0.27; 0.38)	0.002

For further information, see Abbreviations used in this paper and the text. Medians, and 1st and 3rd quartiles (in parentheses) are shown.

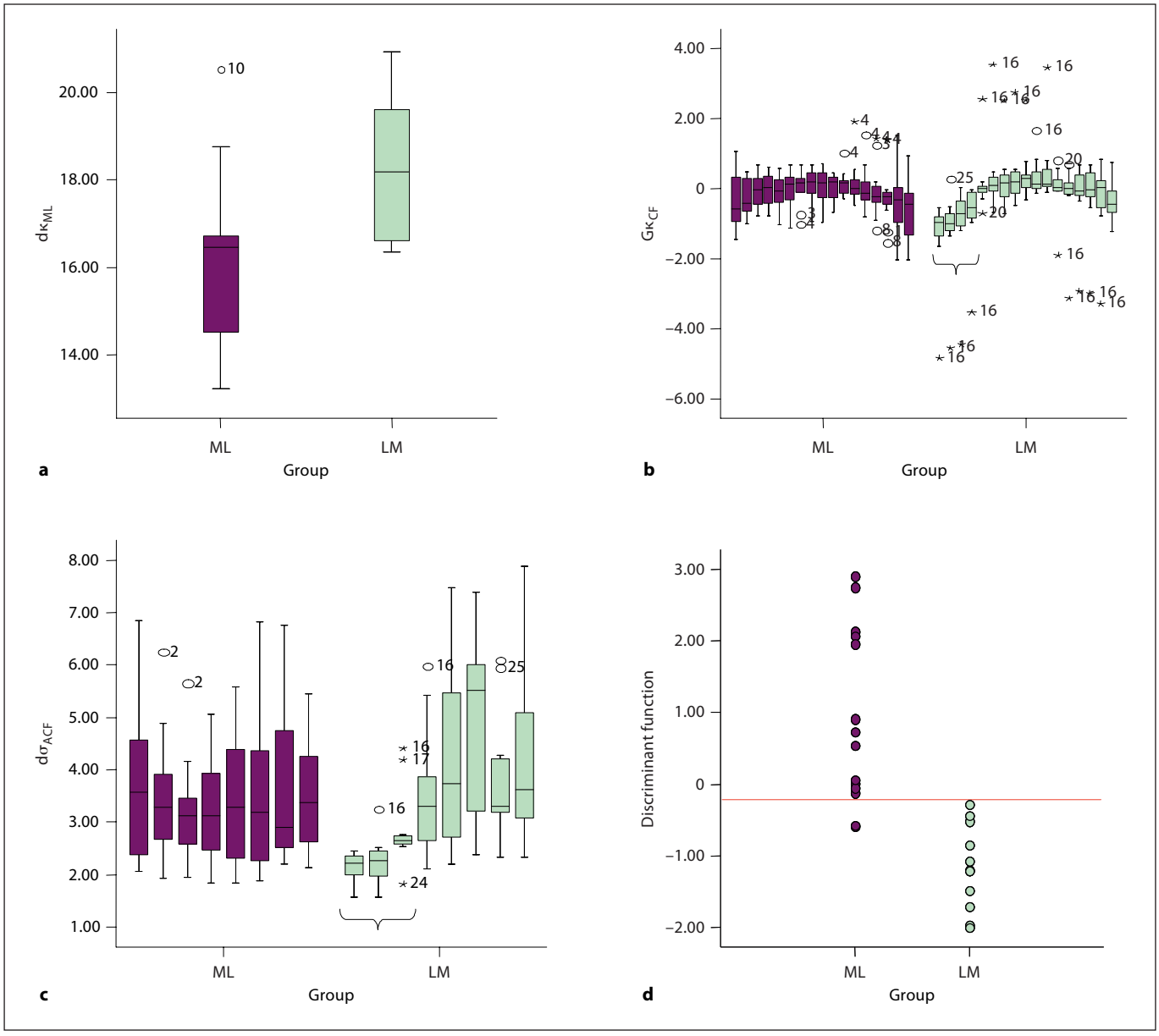

Fig. 6. Graphical representation of the parameters describing TMJ anatomy. **a** Box plot of the distance between the condylar poles $d\kappa_{ML}$ for the ML and LM groups. **b** Incongruence values $G\kappa_{CFi}$ between condyle and fossa in the coronal plane at maximum intercuspation for the ML and LM group; the horizontal brace indicates the four most lateral points of the superior condylar arch closer to the fossa in the LM than in the ML group. **c** Box plot of the distance $d\sigma_{ACF}$ between the condyle and the posterior slope of the eminence; the horizontal brace indicates the three most lateral sections of the superior condylar contour closer to the fossa in the LM than in the ML group. **d** Distribution of the classification function of the multivariate discriminant analysis for the ML and LM groups; the 2 cases of the ML group incorrectly assigned to the LM group are below the red horizontal line.

tween the condylar poles ($d\kappa_{ML}$) is box plotted in figure 6a (the single values are listed in table 1). The distance was significantly smaller (p = 0.035; approximately 2 mm) in the ML (16.3 ± 2.0 mm) than in the LM group (18.2 ± 1.8 mm). In the *coronal plane* κ the maximum curvature of the condyle ($C\kappa_{Cmax}$) did not significantly differ between the ML and LM groups. This was also the case for the incongruence between condyle and fossa in the medial and central parts ($G\kappa_{CFM}$ and $G\kappa_{CFC}$) but not in the lateral part ($G\kappa_{CFL}$). The incongruence values were sig-

Table 3. Classification of stress field paths according to TMJ morphology parameters ($G\kappa_{CF\,17}$, $d\sigma_{ACFmin}$ and $C\sigma_{Pmax}$): 92% of cases correctly classified

	Geometric classification	
	ML (n = 14)	LM (n = 11)
Predicted by discriminant analysis		
ML	12 (85.7%)	0 (0.0%)
LM	2 (14.3%)	11 (100.0%)

nificantly closer to 0 in the ML than in the LM group (p = 0.003), indicating a smaller distance of the condyle to the fossa in the lateral part of the joint for the LM group (fig. 6b). In the *transversal plane* τ the maximum curvature of the anterior condylar arch ($C\tau_{Amax}$) did not significantly differ between the ML and LM groups. Over all *sagittal sections,* the condyles in the LM group were closer to the posterior slope of the eminence in the lateral part of the joint ($d\sigma_{ACFL}$; around 1 mm) than in the ML group (p = 0.004; fig. 6c). Also in the sagittal sections, the condyles in the ML group were more curved anteriorly ($C\sigma_{Amax}$) than the ones in the LM group (p = 0.002). No significant differences in the average fossa steepness ($S\sigma_{avg}$) were found between the ML and LM groups. Multivariate discriminant analysis (jackknifed) was able to assign 92% of the TMJs to the correct stress field path group only by using (a) the coronal incongruence between condyle and fossa of the most lateral joint part ($G\kappa_{CF\,17}$), (b) the minimum distance between the condyle and the posterior slope of the eminence ($d\sigma_{ACFmin}$) and (c) the maximum posterior condylar curvature in the sagittal sections ($C\sigma_{Pmax}$). The parameter mostly contributing to group separation was $G\kappa_{CF\,17}$, the least contributing was $C\sigma_{Pmax}$. If only the first two parameters were used for classification, the correct classification rate decreased slightly to 88%. Figure 6d shows the distribution of the classification function for the ML and LM groups where the 2 cases of the ML group incorrectly classified are visible – almost superimposed – below the horizontal red line.

Discussion

This study was a first attempt at analyzing which aspects of the TMJ morphology might explain different stress field patterns. In former studies, stress fields have been shown to translate perpendicularly to the TMJ disk fibers with a great variability in energy expenditure for cartilage deformation (plowing effect) [Gallo et al., 2000b; Gossi et al., 2004]. Higher energy density localized in areas prone to disk failure [Oberg et al., 1971; Stratmann et al., 1996] would suggest a mechanical wear of the tissues. Thus, TMJ morphologies more likely to concentrate higher energy densities in these areas could help identifying subjects at risk of cartilage lesions.

It has to be noted that this study focused neither on the classification criteria for the stress field paths – which are the topic of another study – nor on the distribution of the patterns across genders. For this analysis, care was taken to have a balanced sample of TMJs from both types, i.e. with stress field trace with ML and LM patterns at jaw opening. Since the data had already been collected, it was not possible to balance the genders between the two groups, females being more represented in the ML group and males more represented in the LM group. Since mandibular anatomy in our patient groups is larger in males than in females we decided to leave out condylar width for further analysis and classification. Morphological analysis is a complex issue that requires first a meticulous visual observation in order to first assess quantitatively common aspects and differences in shape. For this reason, reference planes were defined that would be mostly insensitive to the anatomical variability in human TMJs, as observed in the present data and a previously published study [Anagnostopoulou and Venieratos, 1986]. One further issue is that a quantitative geometric description of anatomical objects can generate a plethora of punctual parameters that demand data reduction. This study has therefore been performed with a limited number of parameters that were supposed to be anatomically meaningful and sufficiently robust for statistical analysis. This data reduction provided some statistically significant differences in the TMJ morphology of both groups: (a) in the LM group the condyle was closer to the fossa in the lateral part both in the coronal as well as sagittal plane whereas (b) in the ML group the condyles were more curved anteriorly. The second finding might indicate frontally more convex condyles in the ML group and flatter ones in the LM group. The condyles being laterally closer to the fossa in the LM group might be due to several reasons, e.g. a thinner or deformed disk, a condyle being thicker laterally than medially (fig. 7) or a stronger angulation of the main condylar axis in ML direction. A thinner or deformed disk might prelude abnormal conditions [Chen et al., 2002] but cannot be demonstrated by the data presently available. A condyle whose dimensions in dorsoventral direction are larger in the lateral part

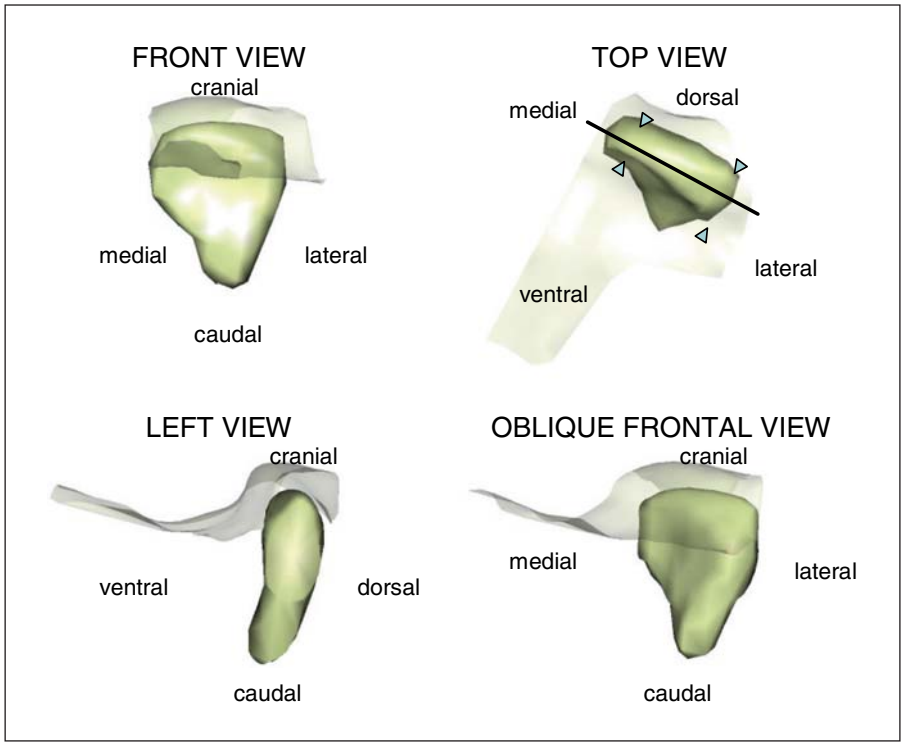

Fig. 7. Example of a TMJ of the LM type (subject No. 16, left TMJ No. 25). In the top view a thick black line represents the main condylar axis and the blue arrowheads show the thickness of the medial and lateral part of the condyle. Note how the lateral part of the condyle is thicker and closer to the fossa.

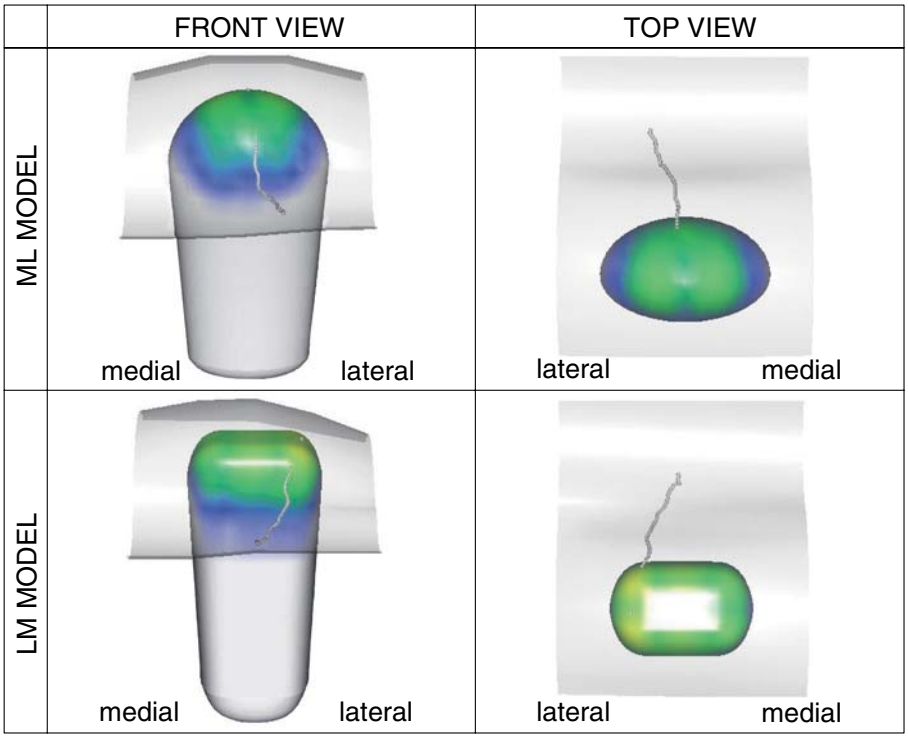

Fig. 8. Models of TMJs simulated according to the morphometric parameters that most characterize the two types of stress field paths. The joint of the ML type was constructed with a rounded condyle and a symmetric fossa. The joint of the LM type was constructed with a more cylindrical condyle and the fossa closer to it laterally. Both joints were moved with identical kinematics: the motion occurred only in the sagittal plane and the main condylar axes were angulated at 15° relative to the transversal direction.

than in the medial part could reduce the lateral joint space more than a cylindrically shaped condyle. This could also happen if the main condylar axis forms a larger angle with the ML direction. With the present techniques, we do not know whether these findings might be due to remodeling or other reasons. The significant differences found in the parameters appear not to be due to methodological bias, such as the side of jaw tracking or any other type of measurement asymmetry for example. As a matter of fact, jaw tracking had always been performed ipsilaterally to the joint analyzed, and the stress field patterns found were of the same type (and therefore symmetrical) in both joints of all but 1 subject studied bilaterally (table 1). Furthermore, there were no side differences in the parameters of the subjects recorded bilaterally as checked by a Wilcoxon signed rank test ($p > 0.05$). Multivariate discriminant analysis permits the determination of the parameters that mostly contribute to case classification. For the sample analyzed, a 92% separation of the two groups was obtained. Also, of interest, the incongruence between condyle and fossa in the most lateral part of the joints ($G\kappa_{CF\,17}$) and the closest condyle-fossa distance $d\sigma_{\mathrm{ACFmin}}$ mostly contributed to this classification. This is a further confirmation that the two stress field pattern groups are mostly discriminated by the location of the minimum joint space. Not considering the third parameter that describes the posterior aspect of the condyle does not have a strong influence on the rate of correct classification (92%) by lowering it by 1 subject to 88%. In order to check the morphological meaning of our findings, we constructed two TMJ models according to the morphometric parameters in the ML and LM groups (fig. 8). The TMJ of the ML type was modeled with a rounded condyle and a relatively flat fossa, whereas the TMJ of the LM type was modeled with a more cylindrical condyle, therefore flatter, and a deeper fossa, in particular with closer distance to the condyle in the lateral part. The jaw opening/closing movement imposed identically on each condyle was constructed as a standard symmetric rotation/translation according to the typical patterns of asymptomatic subjects [Merlini and Palla, 1988], with the paths of the incisors and of the condylar center lying on circular arcs in the sagittal plane. The main condylar axes were angulated at 15° relative to the transversal direction. Thereafter, the stress field paths were calculated as in former studies. In figure 8 one can observe how the stress field paths tend to be similar to those observed in vivo. The TMJ model of the ML type had a stress field pattern running from the middle to the lateral side of the joint during jaw opening and the model of the LM type having a stress field path running from the lateral part of the joint towards the middle. Therefore, it seems that the morphometric parameters are an important factor that can differentiate between the two different stress field patterns.

One obvious limitation of this study is the rather low number of joints examined due to the relative complexity for data acquisition. Furthermore, the morphometric parameters were determined only for the static position of the joints without taking kinematics into account. However, the high degree of separation of the two groups as well as the high significance of some parameters seem to indicate that joint morphology – and therefore growth and remodeling – may play an important role in the areas that are more loaded. Prospective studies are nevertheless needed to show the validity of joint classifications. Furthermore, studies on joint loading related to joint kinematics will also elucidate the role of the quality of mandibular motion in joint loading.

Acknowledgment

This work was supported by grant No. 325200-110067 from the Swiss National Science Foundation, Berne, Switzerland.

References

Airoldi, G.B. (1994) Three-Dimensional Description of Mandibular Finite Helical Axis Pathways in Asymptomatic Subjects; thesis, University of Zürich.

Airoldi, R.L., L.M. Gallo, S. Palla (1994) Precision of the jaw tracking system JAWS-3D. J Orofac Pain *8:* 155–164.

Anagnostopoulou, S., D. Venieratos (1986) Quantitative method for the classification of human mandibular condyles. Acta Anat (Basel) *127:* 201–204.

Andriacchi, T.P., P.L. Lang, E.J. Alexander, D.E. Hurwitz (2000) Methods for evaluating the progression of osteoarthritis. J Rehabil Res Dev *37:* 163–170.

Andriacchi, T.P., C.O. Dyrby, T.S. Johnson (2003) The use of functional analysis in evaluating knee kinematics. Clin Orthop Relat Res *410:* 44–53.

Andriacchi, T.P., A. Mundermann, R.L. Smith, E.J. Alexander, C.O. Dyrby, S. Koo (2004) A framework for the in vivo pathomechanics of osteoarthritis at the knee. Ann Biomed Eng *32:* 447–457.

Ateshian, G.A., S.D. Kwak, L.J. Soslowsky, V.C. Mow (1994) A stereophotogrammetric method for determining in situ contact areas in diarthrodial joints, and a comparison with other methods. J Biomech *27:* 111–124.

Beatty, M.W., M.J. Bruno, L.R. Iwasaki, J.C. Nickel (2001) Strain rate dependent orthotropic properties of pristine and impulsively loaded porcine temporomandibular joint disk. J Biomed Mater Res *57:* 25–34.

Beek, M., J.H. Koolstra, L.J. van Ruijven, T.M. van Eijden (2001) Three-dimensional finite element analysis of the cartilaginous structures in the human temporomandibular joint. J Dent Res *80:* 1913–1918.

Chen, Y.J., L.M. Gallo, S. Palla (2002) The mediolateral temporomandibular joint disc position: an in vivo quantitative study. J Orofac Pain *16:* 29–38.

Fujikawa, K., B.B. Seedhom, V. Wright (1983) Biomechanics of the patello-femoral joint. Part I: A study of the contact and the congruity of the patello-femoral compartment and movement of the patella. Eng Med *12:* 3–11.

Fushima, K., L.M. Gallo, M. Krebs, S. Palla (2003) Analysis of the TMJ intraarticular space variation: a non-invasive insight during mastication. Med Eng Phys *25:* 181–190.

Gallo, L.M., G.B. Airoldi, R.L. Airoldi, S. Palla (1997) Description of mandibular finite helical axis pathways in asymptomatic subjects. J Dent Res *76:* 704–713.

Gallo, L.M., K. Fushima, S. Palla (2000a) Mandibular helical axis pathways during mastication. J Dent Res *79:* 1566–1572.

Gallo, L.M., J.C. Nickel, L.R. Iwasaki, S. Palla (2000b) Stress-field translation in the healthy human temporomandibular joint. J Dent Res *79:* 1740–1746.

Gallo, L.M., D. Gossi, S. Palla (2001) Characterization of stress-field paths in asymptomatic TMJs. J Dent Res *80(SI):* 534.

Gossi, D.B., L.M. Gallo, E. Bahr, S. Palla (2004) Dynamic intra-articular space variation in clicking TMJs. J Dent Res *83:* 480–484.

Hirose, M., E. Tanaka, M. Tanaka, R. Fujita, Y. Kuroda, E. Yamano, T.M. van Eijden, K. Tanne (2006) Three-dimensional finite-element model of the human temporomandibular joint disc during prolonged clenching. Eur J Oral Sci *114:* 441–448.

Krebs, M., L.M. Gallo, R.L. Airoldi, S. Palla (1995) A new method for three-dimensional reconstruction and animation of the temporomandibular joint. Ann Acad Med Singapore *24:* 11–16.

Krebs, M. (1997) Dynamic Stereometry of the Temporomandibular Joint from 3D Imaging and Tracking Data; thesis, ETH Zürich.

Krogh-Poulsen, W. (1973) Die klinische Untersuchung und Befundaufnahme am Kiefergelenkpatienten durch den Zahnarzt; in: Okklusion und Kiefergelenk. Proceedings of the SSO-Fortbildungskurs. Bern, Switzerland, pp 110–118.

Linn, F.C. (1967) Lubrication of animal joints. I. The arthrotripsometer. J Bone Joint Surg Am *49:* 1079–1098.

Merlini, L., S. Palla (1988) The relationship between condylar rotation and anterior translation in healthy and clicking temporomandibular joints. Schweiz Monatsschr Zahnmed *98:* 1191–1199.

Mesqui, F., F. Kaeser, P. Fischer (1986) On-line three-dimensional light spottracker and its application to clinical dentistry. Int Arch Photogrammetry Remote Sensing *26:* 310–317.

Nickel, J.C., K.R. McLachlan (1994a) An analysis of surface congruity in the growing human temporomandibular joint. Arch Oral Biol *39:* 315–321.

Nickel, J.C., K.R. McLachlan (1994b) In vitro measurement of the frictional properties of the temporomandibular joint disc. Arch Oral Biol *39:* 323–331.

Nickel, J.C., K.R. McLachlan (1994c) In vitro measurement of the stress-distribution properties of the pig temporomandibular joint disc. Arch Oral Biol *39:* 439–448.

Nickel, J.C., L.R. Iwasaki, D.E. Feely, K.D. Stormberg, M.W. Beatty (2001) The effect of disc thickness and trauma on disc surface friction in the porcine temporomandibular joint. Arch Oral Biol *46:* 155–162.

Oberg, T., G.E. Carlsson, C.M. Fajers (1971) The temporomandibular joint. A morphologic study on a human autopsy material. Acta Odontol Scand *29:* 349–384.

Palla, S. (1986) New knowledge and methods in the diagnosis of functional disorders of the masticatory system (in German). Schweiz Monatsschr Zahnmed *96 Spec No:* 1329–1351.

Palla, S., L.M. Gallo, D. Gossi (2003) Dynamic stereometry of the temporomandibular joint. Orthod Craniofac Res *6(suppl 1):* 37–47.

Rao, V.M., A. Babaria, A. Manoharan, S. Mandel, N. Gottehrer, H. Wank, S. Grosse (1990) Altered condylar morphology associated with disc displacement in TMJ dysfunction: observations by MRI. Magn Reson Imaging *8:* 231–235.

Salaorni, C., S. Palla (1994) Condylar rotation and anterior translation in healthy human temporomandibular joints. Schweiz Monatsschr Zahnmed *104:* 415–422.

Stratmann, U., K. Schaarschmidt, P. Santamaria (1996) Morphometric investigation of condylar cartilage and disc thickness in the human temporomandibular joint: significance for the definition of ostearthrotic changes. J Oral Pathol Med *25:* 200–205.

Tanaka, E., R. del Porzo, M. Tanaka, D. Asai, M. Hirose, T. Iwabe, K. Tanne (2004) Three-dimensional finite element analysis of human temporomandibular joint with and without disc displacement during jaw opening. Med Eng Phys *26:* 503–511.

Waldman, S.D., J.T. Bryant (1997) Dynamic contact stress and rolling resistance model for total knee arthroplasties. J Biomech Eng *119:* 254–260.